

1 **Evolution of the complex refractive index in the UV spectral region in ageing**  
2 **secondary organic aerosol**

3 **J.M. Flores<sup>1</sup>, D. F. Zhao<sup>2</sup>, L. Segev<sup>1</sup>, P. Schlag<sup>2</sup>, A. Kiendler-Scharr<sup>2</sup>, H. Fuchs<sup>2</sup>, Å. K.**  
4 **Watne<sup>3</sup>, N. Bluvshstein<sup>1</sup>, Th. F. Mentel<sup>2</sup>, M. Hallquist<sup>3</sup>, Y. Rudich<sup>1,\*</sup>**

5 <sup>1</sup>Weizmann Institute of Science, Department of Earth and Planetary Sciences, Rehovot 76100,  
6 Israel

7 <sup>2</sup>Institut für Energie und Klimaforschung: Troposphäre (IEK-8), Forschungszentrum Jülich,  
8 Jülich, D-52425, Germany

9 <sup>3</sup>Dept. of Chemistry and Molecular Biology, Atmospheric Science, University of Gothenburg,  
10 41296 Gothenburg, Sweden

11  
12 \* Correspondence: [yinon.rudich@weizmann.ac.il](mailto:yinon.rudich@weizmann.ac.il)

13  
14 **Abstract**

15  
16 The chemical and physical properties of secondary organic aerosol (SOA) formed by the  
17 photochemical degradation of biogenic and anthropogenic volatile organic compounds (VOC)  
18 are yet poorly constrained. The evolution of the complex refractive index (RI) of SOA, formed  
19 from purely biogenic VOC and mixtures of biogenic and anthropogenic VOC was studied over a  
20 diurnal cycle in the SAPHIR photochemical outdoor chamber in Jülich, Germany. The  
21 correlation of RI with SOA chemical and physical properties such as oxidation level and  
22 volatility was examined. The RI was retrieved by a newly developed broadband cavity enhanced  
23 spectrometer for aerosol optical extinction measurements in the UV spectral region (360 to 420  
24 nm). Chemical composition and volatility of the particles were monitored by a high resolution  
25 time of flight aerosol mass spectrometer, and a volatility tandem differential mobility analyzer.  
26 SOA was formed by ozonolysis of either (i) a mixture of biogenic VOC ( $\alpha$ -pinene and  
27 limonene), (ii) biogenic VOC mixture with subsequent addition of an anthropogenic VOC (p-  
28 xylene-d<sub>10</sub>), or (iii) a mixture of biogenic and anthropogenic VOC. The SOA aged by ozone/OH  
29 reactions up to 29.5 hours was found to be non-absorbing in all cases. The SOA with p-xylene-  
30 d<sub>10</sub> showed an increase of the scattering component of the RI correlated with an increase of the  
31 O/C ratio and with an increase in the SOA density. There was a greater increase in the scattering  
32 component of the RI when the SOA was produced from the mixture of biogenic VOCs and  
33 anthropogenic VOC than from the sequential addition of the VOCs after the approximate same  
34 ageing time. The increase of the scattering component was inversely correlated with the SOA  
35 volatility. Two RI retrievals determined for the pure biogenic SOA showed a constant RI for up  
36 to 5 h of ageing. Mass spectral characterization shows the three types of the SOA formed in this  
37 study have significant amount of semivolatile components. The influence of anthropogenic  
38 VOCs on the oxygenated organic aerosol, and the atmospheric implications are discussed.

## 1 **1 Introduction**

2

3 The interaction between aerosols and incoming solar radiation plays an important role in the  
4 radiative balance of Earth's atmosphere. Aerosols containing light-absorbing carbonaceous  
5 species are a major contributor to the direct and indirect effects on the climate system (Koren et  
6 al., 2008; Andreae and Ramanathan, 2013; Bond et al., 2013). Black carbon, which is the  
7 dominant absorber of solar radiation in the atmosphere, has fairly well defined optical properties  
8 with an estimate of the industrial-era mean direct radiative forcing of approximately  $+1.1 \text{ W m}^{-2}$   
9 (Bond et al., 2013). However, the optical properties of light-absorbing organic particles, or  
10 "brown" carbon (Andreae and Gelencsér, 2006), which may account for 10–40% of the total  
11 light absorption in the atmosphere, and on snow and ice (Park et al., 2010; Bahadur et al., 2012;  
12 Cappa et al., 2012; Chung et al., 2012; Kirchstetter and Thatcher, 2012; Feng et al., 2013; Bond  
13 et al., 2013), are still poorly constrained. Recent studies estimate the global radiative forcing of  
14 brown carbon to be  $0.10\text{--}0.25 \text{ W m}^{-2}$ , with higher values on regional scales (Bond et al., 2013;  
15 Feng et al., 2013). Brown carbon is mainly produced by combustion sources, especially biomass  
16 burning, but it was hypothesized that it can also be produced by atmospheric chemical reactions;  
17 for example in the formation of secondary organic aerosols (SOA). SOA can account for 71% of  
18 the total organic aerosol (OA) sources, and up to 85% when ageing of primary to secondary OA  
19 is included (Spracklen et al., 2011). It is presumed that as SOA ages in the atmosphere, high  
20 molecular weight compounds can form, subsequently enhancing light absorption. For example,  
21 Lambe et al. (2013) showed that the mass absorption coefficient (MAC) at  $\lambda=405 \text{ nm}$  of SOA  
22 from biogenic and anthropogenic sources oxidized with OH, increases with increasing oxidation  
23 level, but has an overall negligible absorption at  $\lambda=532 \text{ nm}$ .

24 It is important to understand the production of SOA from atmospheric oxidation of  
25 biogenic and anthropogenic volatile organic compounds (VOC). Estimations suggest that  
26 globally SOA is dominated by biogenic VOC precursors (BVOC), resulting in 90% biogenic  
27 SOA (BSOA) and 10% anthropogenic SOA (ASOA) (Hallquist et al., 2009). However, in many  
28 case studies, observations of SOA can only be explained assuming enhancement of SOA  
29 production by anthropogenic influences (Spracklen et al., 2011). Several studies have shown that  
30 the interaction between biogenic volatile organic compounds and anthropogenic VOCs (AVOCs)  
31 can significantly affect the properties of SOA (Kautzman et al., 2010; Glasius et al., 2011; Hoyle

1 et al., 2011; Spracklen et al., 2011; Emanuelsson et al., 2013a). Two recent studies have shed  
2 some light on the chemical behavior of AVOCs and BVOCs. Hildebrandt et al. (2011) studied  
3 the mass yields of SOA formed from mixtures of biogenic and anthropogenic precursors and  
4 found that the yields can be parameterized by assuming a common organic phase for  
5 partitioning, and that the SOA derived from mixtures of AVOC and BVOC (ABSOA) can be  
6 treated as an ideal mixture. Similarly, Emanuelsson et al. (2013a) found that the SOA yields and  
7 oxidation levels can be described as linear combinations of the corresponding properties of the  
8 pure biogenic and anthropogenic systems.

9         The complex refractive index (RI;  $m = n + ik$ ) is one of the intrinsic optical properties of  
10 aerosols. The real ( $n$ ) and imaginary ( $k$ ) parts express the extent of scattering and absorption of  
11 light by the aerosol, respectively. Several studies retrieved SOA refractive indices in the  
12 laboratory (Schnaiter et al., 2003; Yu et al., 2008; Wex et al., 2009; Kim et al., 2010; Lang-Yona  
13 et al., 2010; Nakayama et al., 2010; Redmond and Thompson, 2011; Nakayama et al., 2012; Kim  
14 et al., 2012; Lambe et al., 2013; Kim and Paulson, 2013; Nakayama et al., 2013); however,  
15 recent studies exploring the evolution of the optical properties of SOA formed from mixtures of  
16 AVOCs and BVOCs are not available in the literature. Recently, it became possible to retrieve  
17 the RI of aerosols as a function of wavelength using broadband cavity enhanced spectroscopy  
18 (Washenfelder et al., 2013; Wilson et al., 2013; Zhao et al., 2013). In this paper we report the  
19 evolution of the complex refractive index in the UV spectral region of ABSOA formed from  
20 mixtures of biogenic (a mixture of  $\alpha$ -pinene and limonene) and anthropogenic (p-xylene-d<sub>10</sub>)  
21 precursors at low NO<sub>x</sub> levels, by using the approach described in Washenfelder et al. (2013).  
22 Additionally, we explore the relationship between the SOA oxidation level, H/C ratio and  
23 volatility with the RI, by following the SOA aging process due to OH oxidation reactions in the  
24 outdoor atmospheric simulation chamber SAPHIR over a diurnal cycle.

25

## 26 **2 Experiments, instrumentation, and methods**

27

### 28 **2.1 Experiments**

29

30 The experiments took place in the outdoor atmospheric simulation chamber SAPHIR at the  
31 Forschungszentrum Jülich, in Jülich, Germany. The SAPHIR chamber has been previously

1 described in detail (Bohn et al., 2005; Rohrer et al., 2005); only a short description is given here.  
2 SAPHIR is a double-walled Teflon chamber with a volume of 270 m<sup>3</sup>. It is operated with  
3 synthetic air (Linde Lipur, purity 99.9999%), and kept at a slight overpressure of about 50 Pa. To  
4 maintain the overpressure in the chamber and to compensate for the sampling by the instruments,  
5 a continuous flow of 7 – 9 m<sup>3</sup> h<sup>-1</sup> of synthetic air is maintained throughout the experiments. A  
6 fan is used to ensure mixing of the injected trace gases, and the chamber is equipped with a  
7 Louvre system to either open and expose it to natural sun light or close it to simulate night time  
8 processes.

9 To measure the evolution of the generated SOA, the experiments were performed as  
10 follows: after the chamber was flushed throughout the night, synthetic air with about 40 ppm of  
11 CO<sub>2</sub> was injected into the chamber and the relative humidity was increased to ~75 %. Then the  
12 chosen VOCs were introduced and allowed to mix for approximately 2 hours, followed by  
13 injection of 200 ppb of ozone and opening the roof, which marks the beginning of the  
14 experiment. The SOA was allowed to age for at least 29 hours and only at the end of the  
15 experiment the roof was closed. This allowed simulation of a diurnal cycle through which the  
16 aerosols aged. Three experiments were performed in this study: 1) a mixture of biogenic VOCs,  
17 48 ppb of  $\alpha$ -pinene (Sigma-Aldrich, 80605-1ML,  $\geq 98.5\%$ ; St. Louis, MO, USA) and 48 ppb of  
18 limonene (Sigma-Aldrich, 62118,  $\geq 99\%$ ) were added as precursors with an initial OH  
19 concentration of  $7.4 \times 10^6$  cm<sup>-3</sup>, referred to as the BVOC experiment; 2) a sequential addition to  
20 the BVOC mixture of 39 ppb of  $\alpha$ -pinene and 39 ppb of limonene followed by 51 ppb of p-  
21 xylene-d<sub>10</sub> (Sigma-Aldrich, 175927-5G, 99 atom % D) added 5 h after the BVOCs, with an  
22 initial OH concentration of  $7.8 \times 10^6$  cm<sup>-3</sup>, referred to as the sequential experiment; and 3) a  
23 mixture of 42 ppb of  $\alpha$ -pinene, 42 ppb of limonene, and 90 ppb of p-xylene-d<sub>10</sub> were added as  
24 precursors with an OH concentration of  $8.0 \times 10^6$  cm<sup>-3</sup>, referred to as the mixture experiment. The  
25 three experiments performed are summarized in Table 1, and Fig. 1 shows a schematic of the  
26 experimental procedure.

27

## 28 **2.2 Analytical instrumentation**

29

30 The SAPHIR chamber was equipped with temperature, water content, O<sub>3</sub>, NO, and NO<sub>2</sub>  
31 monitors. NO and NO<sub>2</sub> measurements were performed with a chemiluminescence analyzer (Eco

1 Physics AG, TR480, Duerten, Switzerland) equipped with a photolytic converter (Eco Physics  
2 AG, PLC760). Ozone was measured by a UV absorption spectrometer (ANSYCO GmbH, Model  
3 O341M, Karlsruhe, Germany). The detection limit and accuracy were 0.5 ppbv and 5%,  
4 respectively. Hydroxyl radical (OH) concentrations were measured using Laser induced  
5 fluorescence (LIF). The uncertainty of the OH measurement, determined by the accuracy of the  
6 calibration of the LIF instrument, is 10% ( $1\sigma$ ). The LIF instrument is described in detail by  
7 Fuchs et al. (2012). The OH radicals in these experiments are predominantly formed from the  
8 ozonolysis of the VOCs, and to a minor extent by HONO and ozone photolysis (Rohrer et al.,  
9 2005). The absolute water content was measured with a cavity ring down Picarro analyzer  
10 (Picarro G2380, Santa Clara, CA, U.S.A), and was used to calculate the relative humidity. A  
11 spectral radiometer (Bohn et al., 2005) was used to measure the actinic flux, the VOCs'  
12 concentrations were monitored by a PTR-MS (Jordan et al., 2009), and the total particle  
13 concentration and number size distributions were measured by a condensation particle counter  
14 (UWCPC, Model 3786, TSI Inc., Shoreview, MN, USA) and a scanning mobility particle sizer  
15 (SMPS, TSI 3081 and TSI 3786). Fig. 2 shows the time series for the different chamber variables  
16 measured for each of the three experiments. The  $\text{NO}_x$  data is not shown as it was within or below  
17 detection limit for all experiments.

18

### 19 **2.3 Measurement of SOA chemical composition**

20

21 The chemical composition of the SOA was measured with a High-Resolution Time-of-Flight  
22 Aerosol Mass Spectrometer (HR-ToF-AMS, Aerodyne Research Inc., Billerica, MA, U.S.A)  
23 (DeCarlo et al., 2006) operated alternatingly between the MS and PToF-mode. The MS mode (in  
24 which the ion signals are integrated over all particle sizes) was used to determine the SOA  
25 composition. The degree of oxidation of the SOA was characterized by deriving the O/C and  
26 H/C ratios (Aiken et al., 2007; Aiken et al., 2008), and by determining the ratios  $f_{44}$  and  $f_{43}$   
27 (defined as the fractions of the signal at  $m/z = 44$  and  $43$  of the total organics measured by the  
28 AMS) and applying them as suggested by Ng et al. (2010). The corrections for the errors due to  
29 gaseous components preceded the calculation of the O/C ratio,  $f_{44}$  and  $f_{43}$  according to the  
30 generalized method by Allan et al. (2004).

1 The density ( $\rho$ ) of the particles, assuming that they are spherical, was calculated using eq.  
2 1 (DeCarlo et al., 2004):

$$\rho = \frac{d_{va}}{d_m} \rho_o \quad (1)$$

4  
5 where  $d_{va}$  is the vacuum aerodynamic diameter (obtained from the particle time-of-flight  
6 measurements from the TOF-AMS),  $d_m$  is the mode mobility diameter from the SMPS size  
7 distributions, and  $\rho_o$  is the standard density. Calculations of the density are only presented up to  
8 15 h after the experiments began, after that time the vacuum aerodynamic diameter  
9 determination became less accurate, probably due to low particle concentrations, and  
10 consequently the  $\rho$  values became unrealistically variable. However, we do not expect the  
11 density trends and values to change significantly after this point.

#### 12 13 **2.4 Measurement of SOA volatility**

14  
15 The volatility of the SOA was determined with a Volatility Tandem Differential Mobility  
16 Analyzer (VTDMA), see Jonsson et al. (2007) and Salo et al. (2011) for details. The VTDMA  
17 consisted of a Differential Mobility Analyzers (DMA, TSI 3081), eight temperature controlled  
18 ovens, and an SMPS (TSI 3081, TSI 3022). First, a narrow particle size distribution was chosen  
19 with the first DMA, then the size selected aerosol was directed through one of the eight  
20 temperature controlled oven units under laminar flow conditions, and finally classified with the  
21 SMPS. To prevent re-condensation of evaporated gases, activated charcoal diffusion scrubbers  
22 were used at the exit of the ovens. Each heated oven consists of a 50 cm diameter stainless steel  
23 tube mounted on an aluminum block with a heating element set independently to temperature  
24 values between 298 to 563K  $\pm$ 0.1 K. The sample flow of 0.3 lpm was switched between the  
25 ovens yielding a residence time in the heated part of the oven of 2.8 s. The aerosol volume  
26 fraction remaining (VFR) was calculated assuming spherical particles (Ofner et al., 2011) for the  
27 range of elevated temperatures. The VFR decreases with increasing temperature and the data was  
28 fitted to a sigmoidal function as has been described by Emanuelsson *et. al.* (2013b). From the  
29 sigmoidal fits it is possible to obtain the temperature where 50% of the particle volume has

1 evaporated,  $T_{VFR0.5}$ .  $T_{VFR0.5}$  was determined every two hours for each experiment, for particles  
2 with 100 nm diameter for the first six hours, and 200 nm diameter for the remaining time.

3

## 4 **2.5 Measurement of SOA optical properties**

5

6 A dual channel Broadband Cavity Enhanced Spectrometer (BBCES) was used to measure the  
7 aerosol optical extinction and retrieve the complex refractive indices between 360 and 420 nm  
8 (at 0.5 nm resolution). This instrument follows the design described in Washenfelder et al.  
9 (2013), and only a brief description and main differences are given here. The BBCES consist of  
10 two optical cavities and a CPC (TSI 3575) connected in series. One channel covers the 360–390  
11 nm and the other covers the 390–420 nm spectral ranges. Incoherent light emitted from two  
12 LEDs with center wavelengths of 370.2 (M365L2, Thorlabs, Newton, NJ, USA) and 407.1 nm  
13 (M405L2, Thorlabs) is coupled into each optical cavity with two highly reflective plano-concave  
14 mirrors (Advanced Thin Films) situated opposite of each other. The light exiting the cavity is  
15 coupled into an optical fiber and transmitted to a 164 mm focal length Czerny-Turner  
16 spectrometer (Shamrock SR-163, Andor Technology, Belfast, UK) with a cooled CCD array  
17 detector (DU920P-BU, Andor Technology). The spectrometer was calibrated by a reference  
18 Hg/Ar lamp. The extinction coefficient ( $\alpha_{ext}$ ) of the aerosol is determined from the change in  
19 light intensity of the filled cavity relative to a particle-free cavity; taking into account the mirror  
20 reflectivity and the Rayleigh scattering of the carrier gas (Washenfelder et al., 2013).

21 It has been previously shown that by measuring several particle diameters (assuming the  
22 composition of each selected diameter to be the same) and fitting a theoretical Mie curve to the  
23 measured extinction cross sections at a specific wavelength, the RI of the aerosol can be  
24 retrieved (Pettersson et al., 2004; Lack et al., 2006; Abo Riziq et al., 2007; Lang-Yona et al.,  
25 2009; Miles et al., 2010; Bluvshstein et al., 2012; Flores et al., 2012; Washenfelder et al., 2013).  
26 The aerosol optical cross-section,  $\sigma_{ext}$  (cm<sup>2</sup>), is determined by eq. 2:

27

$$\sigma_{ext}(\lambda, D_p, m) = \frac{\alpha_{ext}(\lambda, D_p, m)}{N(D_p)} \quad (2)$$

28

1 where  $\lambda$  is the wavelength of the incidence light,  $D_p$  is the particle mode diameter,  $m$  is the  
2 complex refractive index, and  $N(D_p)$  is the particle number concentration ( $\text{cm}^{-3}$ ). Particles were  
3 size-selected between 175–300 nm in 25nm steps (diameters larger than 250 nm could only be  
4 selected towards the end of the experiments). To measure the optical cross section of the size  
5 selected SOA from the chamber, aerosol from the SAPHIR chamber was sampled at  $1360 \text{ cm}^3$   
6  $\text{min}^{-1}$ , passed through a diffusion dryer ( $\text{RH} < 30\%$ ), size selected with a DMA (TSI 3081) (with  
7 a sheath flow of 11.5 lpm), passed through the BBCES, and counted by the CPC. Each size  
8 selection measurement is an average of 150 spectra integrated for 0.3s. The particle  
9 concentration was corrected for dilution by the BBCES mirror purge flows ( $170 \text{ cm}^3 \text{ min}^{-1}$ ). The  
10 measured extinction cross sections were corrected for multiply charged particles using the closest  
11 measured size distributions from the SMPS connected directly to the SAPHIR chamber and the  
12 Wiedensohler charge distribution parameterization (Wiedensohler, 1988; with subsequent  
13 erratum). Size selection measurements were done, if possible, approximately every two hours  
14 and in parallel with the thermal characterization using the VTDMA. To retrieve the real and  
15 imaginary components of the RI, the retrieval algorithm was limited to search for  $n \geq 1$  and  $k \geq$   
16 0, their physical boundaries.

17

## 18 **3 Results**

19

### 20 **3.1 Refractive indices of SOA from pure BVOC and mixtures of BVOC and AVOC**

21

22 Oxidative ageing can cause changes in the RI of SOA (Liu and Daum, 2008; Cappa et al., 2011;  
23 Nakayama et al., 2012; Lambe et al., 2013; Nakayama et al., 2013), as the chemical speciation,  
24 mean molecular weight, density and polarizability of the SOA change with aging. For all  
25 retrievals in this study, the imaginary part reached zero ( ${}_{-0.00}^{+0.03}$ ) at all wavelengths; in other  
26 words, there was no detectable absorption under the conditions in this study. Consequently, only  
27 the retrieved real part of the RI as a function of wavelength between 360 – 420 nm for the three  
28 different experiments performed are shown in Fig. 3. For clarity, the shown retrieved real parts  
29 are averaged every 1.5 nm and their individual errors not shown, and, for the mixture  
30 experiment, only three out of six retrievals are shown. The averaged errors for the retrievals for



1 each experiment are shown on the left side of each panel (red symbols; their value has no  
2 meaning).

3 Fig. 3a shows the results for the BVOCs experiment with the ageing induced by OH  
4 reactions. Typical  $\text{NO}_x$  levels were  $< 0.3$  ppbv. For comparison, other studies of  $\alpha$ -pinene SOA  
5 ageing by ozone and OH reactions are also included. Fig. 3a shows that there is no  
6 distinguishable change in the RI, within the calculated error, from the two retrievals taken at 2.5  
7 h and 5h after the experiment began. There is only a slight spectral dependence with  $n$  values  
8 varying from  $1.51 (\pm 0.01)$  at  $\lambda = 360\text{nm}$  to  $1.49(\pm 0.01)$  at  $\lambda = 420$  nm. Due to technical problems  
9 only two retrievals could be obtained for this experiment. The results of the sequential  
10 experiment (p-xylene- $\text{d}_{10}$  was added five hours after SOA formation from the  $\alpha$ -pinene and  
11 limonene mixture) are shown in Fig. 3b. For this experiment, the real part increased from a  
12 value of  $n=1.50(\pm 0.01)$  to  $n=1.52(\pm 0.01)$  at  $\lambda=360$  nm, and from  $n=1.45(\pm 0.01)$  to  $n=1.49(\pm 0.02)$   
13 at  $\lambda=420$ , from the first measurement at 4.5 h to 29 h of ageing. Contrary to the BVOC  
14 experiment, there is a clearer increase in the real part. Fig. 3c shows the results for the mixture  
15 experiment (the  $\alpha$ -pinene and limonene mixture and p-xylene- $\text{d}_{10}$  were added simultaneously).  
16 Here there is an increase in the real part of the RI from 1.5 h to 25.2 h of ageing, changing from  
17  $n=1.49(\pm 0.01)$  to  $n=1.54(\pm 0.01)$  at  $\lambda=360$  nm, and from  $n=1.45(\pm 0.01)$  to  $1.49(\pm 0.02)$  at  $\lambda=420$   
18 nm. The three experiments show a slight spectral dependence of the real part of the RI with  
19 higher values of the real part at shorter wavelengths.

20

### 21 **3.2 Refractive indices - literature comparison**

22

23 In the past few years, several laboratory studies have retrieved the complex refractive indices of  
24 SOA generated from biogenic and anthropogenic precursors (Schnaiter et al., 2003; Wex et al.,  
25 2009; Kim et al., 2010; Lang-Yona et al., 2010; Cappa et al., 2011; Kim et al., 2012; Nakayama  
26 et al., 2012; Kim and Paulson, 2013; Lambe et al., 2013; Nakayama et al., 2013), with only a few  
27 retrieving the RIs in the near UV spectral region. For example, for SOA generated from the  
28 ozonolysis of  $\alpha$ -pinene, Liu et al. (2013) found values of the real part of  $n=1.517(\pm 0.003)$  and  
29  $n=1.509(\pm 0.003)$  for  $\lambda=360$  nm and  $\lambda=420$  nm, respectively, using a variable angle spectroscopic  
30 ellipsometer with initial ozone and  $\alpha$ -pinene concentrations of  $52.2 (\pm 2.2)$  ppmv and  $4.0(\pm 1.4)$   
31 ppmv, respectively. The imaginary components they found in this range were below  $k < 10^{-4}$ .

1 Using cavity ring down spectroscopy (CRDS), Nakayama et al. (2012) retrieved values between  
2  $n=1.463(\pm 0.019)$  and  $n=1.475(\pm 0.022)$  at  $\lambda=405$  nm, and Nakayama et al. (2010) found values of  
3  $n=1.458(\pm 0.019)$  at  $\lambda=355$ nm. The imaginary parts for both studies were found to be below  
4 0.003. Both studies used initial concentrations of 0.1 ppmv of  $\alpha$ -pinene, and 1.1 – 2.6 ppmv of  
5 ozone. Wex et al. (2009) retrieved only the real part of the RI by using a white light optical  
6 particle spectrometer, and found a value of  $n=1.45$  for the visible wavelengths. They used O<sub>3</sub>  
7 concentrations of up 2.5 ppmv, and  $\alpha$ -pinene concentrations in excess of that of O<sub>3</sub>. Similarly,  
8 Schnaiter et al. (2003) determined a constant value of  $n=1.44$  for  $\lambda>350$  nm by measuring the  
9 wavelength dependence of the SOA scattering and extinction. They generated the  $\alpha$ -pinene SOA  
10 by admixing 470 ppb ozone, followed by the addition of 61 ppb  $\alpha$ -pinene. Using CRDS and a  
11 photo-acoustic sensor to measure RIs Lambe et al. (2013) found values between  $n = 1.51(\pm 0.02)$   
12 and  $n=1.45(\pm 0.04)$  with imaginary part values of  $k < 0.001$  at  $\lambda=405$  nm for SOA formed by  
13 homogeneous nucleation and condensation following OH oxidation of  $\alpha$ -pinene at different  
14 oxidation levels, using a potential aerosol mass flow tube reactor.

15 For SOA formed by ozonolysis of limonene, we could only find one study that measured  
16 the RI in the UV spectral region. Liu et al. (2013) measured  $n$  values between  $1.520(\pm 0.003)$  and  
17  $1.512(\pm 0.003)$  and imaginary parts below  $k < 10^{-4}$  for wavelengths between 420 and 360 nm.  
18 Recently, Kim and Paulson (2013) measured the real part of the RI for SOA generated from the  
19 ozonolysis of  $\alpha$ -pinene and limonene with and without an OH scavenger in a Teflon chamber  
20 using a polar nephelometer at  $\lambda=532$  nm. For both SOA products, they found that the real part of  
21 the RI increased from  $1.39(\pm 0.03)$  to  $1.52(\pm 0.03)$  as the particles sizes grew in time (up to 4 h),  
22 with no discernible effect when an OH scavenger was used.

23

### 24 **3.3 Relationship between oxidation level and refractive index**

25

26 Oxidative ageing changes the SOA's oxidation state, density, mean molecular weight, and  
27 polarizability (Katrib et al., 2005; Liu and Daum, 2008; Cappa et al., 2011; Lambe et al., 2013).  
28 O/C and H/C ratios are useful metrics to measure the oxidative state of the aerosol (Ng et al.,  
29 2010). Fig. 4 shows the change in the retrieved complex refractive index (real part only) for  
30 wavelengths between 360–420 nm as a function of the O/C ratio (Fig. 4A1, 4B1 and 4C1), H/C

1 ratio (Fig. 4A2, 4B2 and 4C2), and  $T_{VFR\ 0.5}$  (Fig. 4A3, 4B3 and 4C3) as the SOA evolved with  
2 time.

3 It can be seen that for the mixture experiment, the value of the RI increases with SOA  
4 ageing. This is correlated with the SOA increasing oxidation level (Fig. 4C1): the O/C values  
5 increase from  $\sim 0.34 (\pm 0.10)$  at 1.5 h to  $\sim 0.42 (\pm 0.13)$  at 29 h of ageing, the H/C ratio decreases  
6 (Fig. 4C2) from  $\sim 1.55 (\pm 0.16)$  to  $1.49 (\pm 0.15)$ , and the volatility (Fig. 4C3) decreases with  
7  $T_{VFR0.5}$  increasing from  $\sim 366\text{ K } (\pm 2)$  up to  $\sim 388\text{ K } (\pm 1)$ . There is a similar trend for the sequential  
8 experiment. However, the magnitude of the increase in RI with respect to the O/C ratio is  
9 smaller, even though the O/C ratio increased more ( $\sim 0.44$ ) for approximately the same ageing  
10 time. Furthermore, the rate of change of the RI with respect to the H/C ratio is also smaller than  
11 for the mixture experiment: the H/C ratio decreased from around  $1.50 (\pm 0.15)$  to  $\sim 1.45 (\pm 0.15)$ .  
12 There is not a clear difference between the two experiments in the dependence of the real part of  
13 the RI on volatility. For the BVOCs experiment it is difficult to assess a relationship with only  
14 two retrievals within the first 5 h of the experiment. There is only evidence that the RI remained  
15 constant (as seen in Fig. 3) with a small increase in the O/C ratio, and a slight decrease in  
16 volatility with  $T_{VFR0.5}$  increasing from  $365.5\text{ K } (\pm 2.7)$  to  $366.7\text{ K } (\pm 2.6)$ .

17 The relationship between optical properties and chemical composition has been  
18 previously explored. Table 2 summarizes the different studies that have related the RI to the O/C  
19 ratio. Lambe et al. (2013) measured the real part of the RI at  $\lambda = 405\text{ nm}$  for SOA formed from  
20 the OH oxidation of  $\alpha$ -pinene, naphthalene and tricyclo-decane (anthropogenic surrogate  
21 precursors), and guaiacol (biomass burning surrogate precursor). They observed a decrease in  $n$   
22 with increase in SOA oxidation level. For  $\alpha$ -pinene, an O/C=0.42 at the beginning of the  
23 experiment, increasing to an O/C=0.93, and an RI decrease from  $n = 1.51(\pm 0.02)$  to  $1.45(\pm 0.04)$   
24 were obtained. They also observed a slight increase in the imaginary component of the RI from  
25  $k=0$  to  $0.001$ ; however, these values are very low. In contrast, Cappa et al. (2011) who studied  
26 the heterogeneous OH oxidation of squalane (a saturated hydrocarbon) and azelaic acid (a  
27 dicarboxylic acid) particles at  $\lambda=532\text{ nm}$ , observed an increasing trend with similar oxidation  
28 levels (O/C= 0–0.35) compared with the ones measured in this study. They measured an increase  
29 in the real part from about  $n=1.47(\pm 0.02)$  at O/C=0.0 to about  $n=1.52$  at O/C=0.35 for squalene,  
30 and from  $n = 1.46$  to  $1.55$  for azelaic acid at O/C ratios from 0.45 to 0.75. Nakayama et al.  
31 (2013) also saw an increasing trend studying the RI of SOA generated from the photooxidation

1 of toluene (an aromatic hydrocarbon). At  $\lambda=405\text{nm}$  the real part increased from  $n =$   
2  $1.449(\pm 0.030)$  to  $n = 1.567(\pm 0.042)$ , and at  $\lambda=532\text{nm}$  from  $n = 1.431(\pm 0.026)$  to  $n =$   
3  $1.498(\pm 0.025)$  for O/C values from 0.64 to 0.73. Nakayama et al. (2012) retrieved RI values for  
4 SOA produced from the ozonolysis and photooxidation of  $\alpha$ -pinene, and found values from  $n =$   
5  $1.463(\pm 0.019)$  to  $n = 1.475(\pm 0.022)$  at  $\lambda=405\text{ nm}$  and  $n = 1.476(\pm 0.021)$ – $1.458(\pm 0.020)$  at  $\lambda=532$   
6  $\text{nm}$  for O/C ratios from 0.43 to 0.47. Therefore, it is difficult to assess a decreasing or increasing  
7 trend from the Nakayama et al. (2012) study.

8

### 9 **3.4 Chemical ageing**

10

11 To help assess the chemical changes in the different SOA and compare them to literature values,  
12 Fig. 5 shows a van Krevelen diagram (van Krevelen, 1950) of the H/C ratio as a function of the  
13 O/C ratio. Fig. 5a shows that the H/C ratio for the BVOC and sequential experiment show a  
14 similar behavior, the H/C ratio remains nearly constant for the first few hours of the experiment  
15 and then decreases. For the BVOC experiment the H/C ratio starts at around 1.50 and decreases  
16 to about 1.40, and in the sequential experiment begins at 1.51 that decreases to  $\sim 1.43$ . The  
17 mixture experiment, however, shows an increase of the H/C ratio in the first few hours of the  
18 experiment, from 1.51 to 1.57, followed by a decrease to  $\sim 1.49$  at the end of the experiment.

19 In the evolution of the O/C and H/C ratios there are three distinct features: 1) the initial  
20 increase in the H/C ratio, especially seen in the mixture experiment; 2) the increase of the O/C  
21 ratio during day time with the H/C remaining almost constant; and 3) the O/C remaining  
22 constant, even decreasing, during night time while the H/C decreased. The initial increase of the  
23 H/C to O/C ratio occurs in the phase of vigorous chemistry and particle growth at the instance  
24 ozone is added. There are two overlapping processes occurring in this stage: chemical ageing,  
25 which increases the O/C ratio and lowers the H/C ratio (e.g. pinic acid, multiple ketones), and  
26 fast growth by dissolution of semivolatile oxidized products, which maintains the O/C ratio of  
27 the precursors (e.g. pinonic acid, pinonealdehyde, hydroperoxides), but has an increasing effect  
28 on the H/C ratio. The strongest effect in the initial increase of the H/C ratio, with the  
29 simultaneous O/C increase, is clearly seen in the mixture experiment. This may be due to the  
30 oxidation conditions, or it could reflect the influence of p-xylene-d<sub>10</sub>. The difference is not clear  
31 as the three experiments began with similar temperatures, RH values, pressure and OH

1 concentrations (Fig.2). However, the initial ozone concentration and solar radiation exposure  
2 were lower for the mixture experiment than for the other two experiments.

3 Following this initial stage, the mixtures are photochemical aged, with an OH  
4 concentration of about  $2\text{-}3 \times 10^6$  molecules  $\text{cm}^{-3}$  (see Fig. 2 middle panels) for the three  
5 experiments. Here there are slight differences in the O/C values between the BVOC and  
6 sequential experiment. This might be caused by either the addition of p-xylene-d<sub>10</sub> 5h after the  
7 insertion of the  $\alpha$ -pinene-limonene mixture, or the specific oxidation conditions. However, there  
8 were no significant differences between the experimental initial conditions, neither the  
9 meteorological condition nor the VOC and O<sub>3</sub> concentrations.

10 During the night the O/C ratio remained constant, showing a slight decrease in the BVOC  
11 and sequential experiments, while the H/C ratio decreased. The slight decrease of O/C overnight  
12 might be due to reactions in the particulate phase (e.g oligomerization). The observed decrease in  
13 the H/C ratio during the night is probably caused by the dilution flow into the chamber which  
14 depletes the gas phase, including semivolatile oxidized compounds, leading to their evaporation.  
15 The excess of semivolatiles, caused by the high initial load of monoterpenes ceases at the end of  
16 the night and onset of the next day. This is seen by the simultaneous decrease of H/C and O/C; at  
17 this stage the molecules were converted to higher oxidized generations by OH reactions during  
18 the second day.

19

## 20 **4 Discussion**

21

22 By comparing the H/C and O/C ratios measured in this study to values measured in different  
23 cities around the world (Fig. 5b), it is clear that the SOA in this study is less oxidized. The fact  
24 that the SOA is not as oxidized may explain the lack of absorption observed, though Nakayama  
25 et al. (2012) measured similar values of the H/C and O/C ratios and also found negligible  
26 absorption. Cappa et al. (2011) with higher values of the H/C ratio and lower values of the O/C  
27 ratio assumed purely scattering particles. Lambe et al. (2013) which were able to age BSOA  
28 formed from OH oxidation of  $\alpha$ -pinene (Fig. 5b, red triangles) up to an O/C = 0.93 and an  
29 H/C=1.1 only saw an increase in the imaginary component from  $k = 0$  to  $k = 0.001$ . And for  
30 ASOA, formed from the OH oxidation of naphthalene, they saw an increase in  $k$  up to 0.0035 for  
31 an O/C = 1.3 and H/C = 0.84. Only Nakayama et al. (2013) saw slightly higher absorption at O/C

1 ratios between 0.64 – 0.73, but for SOA generated from the photooxidation of toluene at  
2 different NO<sub>x</sub> levels, with measured *k* values between 0.0018(±0.0014) and 0.0072(±0.0010) at λ  
3 = 405 nm.

4 The values of the real part retrieved in this study are within the values reported in the  
5 literature; however, there is a significant span in the real part, from *n*=1.44 to *n*=1.58, among all  
6 the studies (for example, see the values at λ=405nm in Table 2 and Fig.3). The differences in RI  
7 values suggest differences in the SOA chemical composition, which can arise from several  
8 different factors; for example, the initial VOC and its concentration, oxidant levels, formation  
9 temperature and relative humidity, the residence times in either the flow tubes or chamber  
10 experiments, and the experimental procedure. The differences in the SOA chemical composition  
11 from different initial VOC concentration (which will directly influence the initial mass  
12 concentration) seems unlikely; on the one hand, Bateman et al. (2011) and Walser et al. (2008)  
13 demonstrated that the composition of limonene + O<sub>3</sub> SOA formed in either a smog chamber with  
14 low mixing ratios (<0.1 ppmv) or a flow tube with significantly higher (~10 ppmv) mixing  
15 ratios, is similar. On the other hand, Shilling et al. (2009) saw small composition differences of  
16 α-pinene SOA when mass concentrations were above 20 μg m<sup>-3</sup>. All the studies reported here  
17 used mass concentration greater than 20 μg m<sup>-3</sup>; hence, no significant differences in the RIs  
18 would be expected. The oxidation level may perhaps explain the differences; however, there are  
19 no clear trends from the available studies. For example, Lambe et al. (2013) showed that the real  
20 part of the RI decreases with increasing oxidation, and Liu et al. (2013) mentioned that the low  
21 oxidation level of their SOA (from Shilling et al. (2009) this would correspond to an O/C < 0.3  
22 as the mass loading was > 140 μg m<sup>-3</sup>) could possibly explain that their measured *n* values are  
23 higher than the other reported values. In contrast, Cappa et al. (2011) and Nakayama et al. (2013)  
24 observed the opposite trend; i.e., an increase in the real part with increasing O/C ratio, which is  
25 the same trend observed in this study. The initial increase in the real part of the RI in this study  
26 might be explained by the change in the SOA density. One form of the Lorentz-Lorentz relation  
27 associates the RI to the mean polarizability (α), the molecular weight (MW) and the density of  
28 the particle:

29

$$\frac{(n^2 - 1)}{(n^2 + 2)} = \frac{\alpha \cdot \rho}{3 \cdot MW} \quad (5)$$

1  
2 Furthermore, Liu and Daum (2008) showed that the real part of the refractive index increases  
3 with mass density, and Katrib et al. (2005) showed the density of layers of oleic acid increases as  
4 the oxygen content also increases. Fig. 6a shows the change in SOA density with time for the  
5 three experiments; only values up to 15 h after the experiments began are shown, and Fig. 6b  
6 shows the change in RI vs. density. Fig. 6b clearly shows the concomitant increase in the real  
7 part of the RI and density for the sequential and mixture experiments, while Fig. 6a demonstrates  
8 the  $\rho$  increase for all experiments and the distinct differences in change of density with time  
9 among the three experiments. For example, the BVOC experiment shows the lowest values up  
10 until about 14 h after the beginning of the experiment, when it acquires the same values as the  
11 sequential experiment, while the mixture experiment shows consistently higher values than the  
12 BVOC and sequential experiments. The increase in  $\rho$  seen in Fig. 6b can help explain the  
13 increase in the real part of the RI seen in the mixture (Fig. 4C1) and sequential experiments (Fig.  
14 4B1), and assuming the trends between the experiments remain the same up to 30 h after the  
15 experiments began, the greater increase in the RI in the mixture experiment. Fig. 6b also  
16 demonstrates the influence of the MW due to the addition of p-xylene-d<sub>10</sub>, as the initial RI for the  
17 BVOC experiment is higher than the sequential and mixture experiments.

18         The increase in the density from 4.5 h to 7 h after the beginning of the experiment seen in  
19 the sequential experiment occurred practically under dark conditions (see Fig. 2 j(NO<sub>2</sub>) values).  
20 This might be attributed to a combination of a few processes: condensation of ozonolysis  
21 products, oligomerization and evaporation of more volatile material from the particles. Between  
22 4.5 h and 7 h the photochemistry and oxidation of p-xylene-d<sub>10</sub> stopped due to the lack of  
23 sunlight, but O<sub>3</sub> and some monoterpenes were still present. Furthermore, the O/C ratio slightly  
24 decreased in that period. This indicates that either ozonolysis products with smaller O/C ratios  
25 than the products from photo-chemistry condensed onto the SOA, or that non-oxidative liquid  
26 phase processes of glyoxal-like structures (i.e., oligomerization) took place at the same time,  
27 such as condensation reactions that can lower the O/C ratio, but still compact the particles.

28

## 29 **5 Atmospheric relevance and implications**

30

1 To assess the atmospheric relevance of the SOA measured in this study Fig. 7 shows the  $f_{44}$  vs.  
2  $f_{43}$  ratio measured for the three experiments presented here. Ng et al. (2010) suggested that the  
3 ratio  $f_{44}/f_{43}$  can be used to estimate the degree of oxidation and volatility, within the oxygenated  
4 organic aerosol (OOA) components; they defined the less oxidized components (lower  $f_{44}$ ) as  
5 semi-volatile OOA and the more oxidized (higher  $f_{44}$ ) as low-volatility OOA. In other words, a  
6 low  $f_{44}/f_{43}$  value can be used as an indication of semi-volatile OOA and a higher  $f_{44}/f_{43}$  value  
7 indicates lower volatility OOA. The triangle in the insert in Fig. 7 shows the area proposed by  
8 Ng et al. (2010) which encompasses the majority of the OOA measured in the field. It can be  
9 seen that the SOA studied here fall within the lower right section of the triangle and are overall  
10 similar, suggesting that the SOA formed in these experiments may be semi-volatile.  
11 Furthermore, Fig. 7 shows that for all three experiments the  $f_{44}$  signal increases and  $f_{43}$  decreases  
12 as the SOA age, from approximately  $f_{44} = 0.05$  to  $\sim 0.08$  to  $0.10$  and from  $f_{43} = 0.16$  down to  
13  $\sim 0.12$ , confirming that the SOA became less volatile with time, as shown in Figs. 4B3 and 4C3.  
14 Moreover, whereas there is no distinguishable difference in the  $f_{44}/f_{43}$  signals between the  
15 BVOCs and sequential experiment, the mixture experiment has a lower  $f_{43}$  signal at a given  $f_{44}$   
16 suggesting that BSOA have less volatile components ( $f_{43}$ ) than ABSOA at the same degree of  
17 oxidation ( $f_{44}$ ). It further suggests that the interaction of p-xylene-d<sub>10</sub> with  $\alpha$ -pinene and limonene  
18 in the mixture experiment can change the chemical and volatility properties of the ABSOA  
19 formed in comparison to the properties of BSOA; whereas the interaction of p-xylene-d<sub>10</sub> with  
20 BSOA in the sequential experiment does not significantly alter the chemical and volatility  
21 properties. However, overall the mass spectral characteristics do not show enough differences to  
22 distinguish the influence of anthropogenic VOCs on the oxygenated organic aerosol. Fig. 7 also  
23 shows that even though the BSOA and ABSOA were not oxidized significantly and the initial  
24 BVOC and AVOC concentrations are higher than atmospherically relevant concentrations, the  
25 oxidation and volatility levels of the SOA fall within an atmospherically relevant range;  
26 specifically at the edge of large  $f_{43}$ , i.e. there is large influence of semivolatiles.

27

## 28 **6 Conclusions**

29

30 We have measured the evolution of the complex refractive index in the UV spectral region,  
31 between 360 and 420 nm, of BSOA and ABSOA formed from three different mixtures of



1 biogenic (a mixture of  $\alpha$ -pinene and limonene) and anthropogenic (p-xylene-d<sub>10</sub>) VOCs at low  
2 NO<sub>x</sub> levels. Additionally, we have explored the relationship of the oxidation level, H/C, and  
3 volatility with the RI as the SOA ages due to OH oxidation in the outdoor atmospheric  
4 simulation chamber SAPHIR over a diurnal cycle. One experiment consisted of pure BSOA  
5 produced from a 1:1 mixture of  $\alpha$ -pinene and limonene, the other two experiments consisted of  
6 ABSOA, one with the ABSOA produced from the sequential addition of a 1:1 mixture of  $\alpha$ -  
7 pinene and limonene followed by p-xylene-d<sub>10</sub>, and the other with the ABSOA produced from a  
8 mixture of  $\alpha$ -pinene, limonene and p-xylene-d<sub>10</sub>. We found an increase in the real part of the RI  
9 with ABSOA ageing, and no detectable absorption in any of the experiments. Furthermore, we  
10 observed a correlation between the increase in the real part of the RI and the increase of the O/C  
11 ratio, with a greater increase in RI when the ABSOA is produced from the mixture of BVOCs  
12 and AVOC than from the sequential addition of the VOCs after the approximate same ageing  
13 time. This suggests the interaction of BVOCs and AVOCs can make the ABSOA a more  
14 scattering aerosol. The increase in the real part points to the fact that it can be associated with an  
15 increase in the aerosol density. On the other hand, we only have RI retrievals up to 5 h of ageing  
16 for the BSOA and could not assess how much the real part increases, if at all, over a diurnal  
17 cycle. We also observed differences in the volatility and the H/C ratio between the BSOA and  
18 the ABSOA. From analyzing the  $f_{44}$  vs.  $f_{43}$  ratios measured for the three experiments, all three  
19 types of SOA can be considered semi-volatile oxygenated organic aerosols, and it is suggested  
20 that the interaction of AVOC and BVOC can form ABSOA with different chemical and volatility  
21 properties than pure BSOA or BSOA that interacts with AVOC. A caveat with respect to  
22 generalization of the results obtained in this study is that the SOA measured is less oxidized than  
23 SOA measured in different cities around the world. The O/C values in the three experiments  
24 ranged from ~0.35 to 0.44, whereas the ones measured in the field are between 0.54 and 1.02.

25 The results from this study are representative of clean conditions due to the low NO<sub>x</sub>  
26 conditions used. Furthermore, they demonstrate that the optical properties of SOA are influenced  
27 by the interaction of BVOCs and AVOCs, are in continuous evolution, and the magnitude of  
28 their change depends explicitly on the formation mechanism of the SOA.

29  
30 *Acknowledgments.* This study was partially supported by the German-Israeli Foundation for  
31 Scientific Research and Development, Research Grant No. 1136-26.8/2011, by the

1 EUROCHAMP2 transnational access activity E2-2012-04-22-0072, and by FP7-ENV-2010-  
2 265148-PEGASOS. JMF is supported by a research grant from the Jinich Postdoctoral  
3 Fellowship. We thank the SAPHIR team, especially Franz Rohrer, Birger Bohn, Rolf Häsel,er,  
4 Martin Kaminski, Anna Lutz and Ismail-Hakki Acir for providing helpful data and supporting  
5 our measurements. We also thank Steve S. Brown and Rebecca Washenfelder for helpful  
6 discussions and support with the optical system.

7

## 8 **5 References**

- 9 Abo Riziq, A., Erlick, C., Dinar, E., and Rudich, Y.: Optical properties of absorbing and non-  
10 absorbing aerosols retrieved by cavity ring down (CRD) spectroscopy, *Atmos. Chem. Phys.*, 7,  
11 1523-1536, 10.5194/acp-7-1523-2007, 2007.
- 12 Aiken, A.C., DeCarlo, P.F. and Jimenez, J.L.: Elemental Analysis of Organic Species with  
13 Electron Ionization High-Resolution Mass Spectrometry, *Anal. Chem.*, 79, 8350-8358, 2007.
- 14 Aiken, A.C., DeCarlo, P.F., Kroll, J.H., Worsnop, D.R., Huffman, J.A., Docherty, K.S., Ulbrich,  
15 I.M., Mohr, C., Kimmel, J.R., Sueper, D., Sun, Y., Zhang, Q., Trimborn, A., Northway, M.,  
16 Ziemann, P.J., Canagaratna, M.R., Onasch, T.B., Alfarra, M.R., Prevot, A.S.H., Dommen, J.,  
17 Duplissy, J., Metzger, A., Baltensperger, U. and Jimenez, J.L.: O/C and OM/OC Ratios of  
18 Primary, Secondary, and Ambient Organic Aerosols with High-Resolution Time-of-Flight  
19 Aerosol Mass Spectrometry, *Environ. Sci. Technol.*, 42, 4478-4485, 2008.
- 20 Allan, J.D., Delia, A.E., Coe, H., Bower, K.N., Alfarra, M.R., Jimenez, J.L., Middlebrook, A.M.,  
21 Drewnick, F., Onasch, T.B., Canagaratna, M.R., Jayne, J.T. and Worsnop, D.R.: A generalised  
22 method for the extraction of chemically resolved mass spectra from Aerodyne aerosol mass  
23 spectrometer data, *J. Aerosol Sci.*, 35, 909-922, 2004.
- 24 Andreae, M.O. and Gelencsér, A.: Black carbon or brown carbon? The nature of light-absorbing  
25 carbonaceous aerosols, *Atmos. Chem. Phys.*, 6, 3131-3148, 2006.
- 26 Andreae, M.O. and Ramanathan, V.: Climate's Dark Forcings, *Science*, 340, 280-281, 2013.
- 27 Bahadur, R., Praveen, P.S., Xu, Y. and Ramanathan, V.: Solar absorption by elemental and  
28 brown carbon determined from spectral observations, *Proc. Natl. Acad. Sci.*, 109, 17366-17371,  
29 2012.
- 30 Bateman, A.P., Nizkorodov, S.A., Laskin, J. and Laskin, A.: Photolytic processing of secondary  
31 organic aerosols dissolved in cloud droplets, *Phys. Chem. Chem. Phys.*, 13, 12199-12212, 2011.
- 32 Bluvshstein, N., Flores, J.M., Riziq, A.A. and Rudich, Y.: An Approach for Faster Retrieval of  
33 Aerosols' Complex Refractive Index Using Cavity Ring-Down Spectroscopy, *Aerosol Sci. and  
34 Technol.*, 46, 1140-1150, 2012.

- 1 Bohn, B., Rohrer, F., Brauers, T. and Wahner, A.: Actinometric measurements of NO<sub>2</sub>  
2 photolysis frequencies in the atmosphere simulation chamber SAPHIR, *Atmos. Chem. Phys.*, 5,  
3 493-503, 2005.
- 4 Bond, T.C. and Bergstrom, R.W.: Light absorption by carbonaceous particles: An investigative  
5 review, *Aerosol Sci. Technol.*, 40, 27-67, 2006.
- 6 Bond, T.C., Doherty, S.J., Fahey, D.W., Forster, P.M., Berntsen, T., DeAngelo, B.J., Flanner,  
7 M.G., Ghan, S., Kärcher, B., Koch, D., Kinne, S., Kondo, Y., Quinn, P.K., Sarofim, M.C.,  
8 Schultz, M.G., Schulz, M., Venkataraman, C., Zhang, H., Zhang, S., Bellouin, N., Guttikunda,  
9 S.K., Hopke, P.K., Jacobson, M.Z., Kaiser, J.W., Klimont, Z., Lohmann, U., Schwarz, J.P.,  
10 Shindell, D., Storelvmo, T., Warren, S.G. and Zender, C.S.: Bounding the role of black carbon  
11 in the climate system: A scientific assessment, *J. Geophys. Res.- Atmos.*, 118, 5380-5552, 2013.
- 12 Cappa, C.D., Che, D.L., Kessler, S.H., Kroll, J.H. and Wilson, K.R.: Variations in organic  
13 aerosol optical and hygroscopic properties upon heterogeneous OH oxidation, *J. Geophys. Res.-*  
14 *Atmos.*, 116, D15204, 2011.
- 15 Cappa, C.D., Onasch, T.B., Massoli, P., Worsnop, D.R., Bates, T.S., Cross, E.S., Davidovits, P.,  
16 Hakala, J., Hayden, K.L., Jobson, B.T., Kolesar, K.R., Lack, D.A., Lerner, B.M., Li, S.-M.,  
17 Mellon, D., Nuaaman, I., Olfert, J.S., Petäjä, T., Quinn, P.K., Song, C., Subramanian, R.,  
18 Williams, E.J. and Zaveri, R.A.: Radiative Absorption Enhancements Due to the Mixing State of  
19 Atmospheric Black Carbon, *Science*, 337, 1078-1081, 2012.
- 20 Chen, Y. and Bond, T.C.: Light absorption by organic carbon from wood combustion, *Atmos.*  
21 *Chem. Phys.*, 10, 1773-1787, 2010.
- 22 Chung, C.E., Ramanathan, V. and Decremer, D.: Observationally constrained estimates of  
23 carbonaceous aerosol radiative forcing, *Proc. Natl. Acad. Sci.*, 109, 11624-11629, 2012.
- 24 Daumit, K.E., Kessler, S.H. and Kroll, J.H.: Average chemical properties and potential  
25 formation pathways of highly oxidized organic aerosol, *Faraday Discuss.*, 165, 181-202, 2013.
- 26 DeCarlo, P.F., Kimmel, J.R., Trimborn, A., Northway, M.J., Jayne, J.T., Aiken, A.C., Gonin, M.,  
27 Fuhrer, K., Horvath, T., Docherty, K.S., Worsnop, D.R. and Jimenez, J.L.: Field-Deployable,  
28 High-Resolution, Time-of-Flight Aerosol Mass Spectrometer, *Anal. Chem.*, 78, 8281-8289,  
29 2006.
- 30 DeCarlo, P. F., Slowik, J. G., Worsnop, D. R., Davidovits, P., and Jimenez, J. L.: Particle  
31 Morphology and Density Characterization by Combined Mobility and Aerodynamic Diameter  
32 Measurements. Part 1: Theory, *Aerosol Sci. Technol.*, 38, 1185-1205,  
33 10.1080/027868290903907, 2004.
- 34 Donahue, N. M., Henry, K. M., Mentel, T. F., Kiendler-Scharr, A., Spindler, C., Bohn, B.,  
35 Brauers, T., Dorn, H. P., Fuchs, H., Tillmann, R., Wahner, A., Saathoff, H., Naumann, K.-H.,  
36 Möhler, O., Leisner, T., Müller, L., Reinnig, M.-C., Hoffmann, T., Salo, K., Hallquist, M.,  
37 Frosch, M., Bilde, M., Tritscher, T., Barmet, P., Praplan, A. P., DeCarlo, P. F., Dommen, J.,  
38 Prévôt, A. S. H., and Baltensperger, U.: Aging of biogenic secondary organic aerosol via gas-  
39 phase OH radical reactions, *Proc. Natl. Acad. Sci.*, 109, 13503-13508, 2012.

- 1 Emanuelsson, E.U., Hallquist, M., Kristensen, K., Glasius, M., Bohn, B., Fuchs, H., Kammer, B.,  
2 Kiendler-Scharr, A., Nehr, S., Rubach, F., Tillmann, R., Wahner, A., Wu, H.C. and Mentel, T.F.:  
3 Formation of anthropogenic secondary organic aerosol (SOA) and its influence on biogenic SOA  
4 properties, *Atmos. Chem. Phys.*, 13, 2837-2855, 2013a.
- 5 Emanuelsson, E.U., Watne, Å.K., Lutz, A., Ljungström, E. and Hallquist, M.: Influence of  
6 Humidity, Temperature, and Radicals on the Formation and Thermal Properties of Secondary  
7 Organic Aerosol (SOA) from Ozonolysis of  $\beta$ -Pinene, *J. Phys. Chem. A*, 117, 10346-10358,  
8 2013b.
- 9 Feng, Y., Ramanathan, V. and Kotamarthi, V.R.: Brown carbon: a significant atmospheric  
10 absorber of solar radiation?, *Atmos. Chem. Phys.*, 13, 8607-8621, 2013.
- 11 Fuchs, H., Dorn, H.P., Bachner, M., Bohn, B., Brauers, T., Gomm, S., Hofzumahaus, A.,  
12 Holland, F., Nehr, S., Rohrer, F., Tillmann, R. and Wahner, A.: Comparison of OH  
13 concentration measurements by DOAS and LIF during SAPHIR chamber experiments at high  
14 OH reactivity and low NO concentration, *Atmos. Meas. Tech.*, 5, 1611-1626, 2012.
- 15 Glasius, M., la Cour, A. and Lohse, C.: Fossil and nonfossil carbon in fine particulate matter: A  
16 study of five European cities, *J. Geophys. Res.- Atmos.*, 116, D11302, 2011.
- 17 Hallquist, M., Wenger, J.C., Baltensperger, U., Rudich, Y., Simpson, D., Claeys, M., Dommen,  
18 J., Donahue, N.M., George, C., Goldstein, A.H., Hamilton, J.F., Herrmann, H., Hoffmann, T.,  
19 Iinuma, Y., Jang, M., Jenkin, M.E., Jimenez, J.L., Kiendler-Scharr, A., Maenhaut, W.,  
20 McFiggans, G., Mentel, T.F., Monod, A., Prévôt, A.S.H., Seinfeld, J.H., Surratt, J.D.,  
21 Szmigielski, R. and Wildt, J.: The formation, properties and impact of secondary organic  
22 aerosol: current and emerging issues, *Atmos. Chem. Phys.*, 9, 5155-5236, 2009.
- 23 Hildebrandt, L., Henry, K.M., Kroll, J.H., Worsnop, D.R., Pandis, S.N. and Donahue, N.M.:  
24 Evaluating the Mixing of Organic Aerosol Components Using High-Resolution Aerosol Mass  
25 Spectrometry, *Environ. Sci. Technol.*, 45, 6329-6335, 2011.
- 26 Hoyle, C.R., Boy, M., Donahue, N.M., Fry, J.L., Glasius, M., Guenther, A., Hallar, A.G., Huff  
27 Hartz, K., Petters, M.D., Petäjä, T., Rosenoern, T. and Sullivan, A.P.: A review of the  
28 anthropogenic influence on biogenic secondary organic aerosol, *Atmos. Chem. Phys.*, 11, 321-  
29 343, 2011.
- 30 Jonsson, Å.M., Hallquist, M. and Saathoff, H.: Volatility of secondary organic aerosols from the  
31 ozone initiated oxidation of -pinene and limonene, *J. Aerosol Sci.*, 38, 843-852, 2007.
- 32 Jordan, A., Haidacher, S., Hanel, G., Hartungen, E., Märk, L., Seehauser, H., Schotzkowsky, R.,  
33 Sulzer, P. and Märk, T.D.: A high resolution and high sensitivity proton-transfer-reaction time-  
34 of-flight mass spectrometer (PTR-TOF-MS), *Int. J. Mass Spectrom.*, 286, 122-128, 2009.
- 35 Katrib, Y., Martin, S.T., Rudich, Y., Davidovits, P., Jayne, J.T. and Worsnop, D.R.: Density  
36 changes of aerosol particles as a result of chemical reaction, *Atmos. Chem. Phys.*, 5, 275-291,  
37 2005.

- 1 Kautzman, K.E., Surratt, J.D., Chan, M.N., Chan, A.W.H., Hersey, S.P., Chhabra, P.S., Dalleska,  
2 N.F., Wennberg, P.O., Flagan, R.C. and Seinfeld, J.H.: Chemical Composition of Gas- and  
3 Aerosol-Phase Products from the Photooxidation of Naphthalene, *J. Phy. Chem. A*, 114, 913-  
4 934, 2010.
- 5 Kim, H. and Paulson, S.E.: Real refractive indices and volatility of secondary organic aerosol  
6 generated from photooxidation and ozonolysis of limonene,  $\alpha$ -pinene and toluene, *Atmos. Chem.*  
7 *Phys.*, 13, 7711-7723, 2013.
- 8 Kim, H., Barkey, B. and Paulson, S.E.: Real refractive indices of  $\alpha$ - and  $\beta$ -pinene and toluene  
9 secondary organic aerosols generated from ozonolysis and photo-oxidation, *J. Geophys. Res.-*  
10 *Atmos.*, 115, D24212, 2010.
- 11 Kim, H., Barkey, B. and Paulson, S.E.: Real Refractive Indices and Formation Yields of  
12 Secondary Organic Aerosol Generated from Photooxidation of Limonene and  $\alpha$ -Pinene: The  
13 Effect of the HC/NO<sub>x</sub> Ratio, *J. Phys. Chem. A*, 116, 6059-6067, 2012.
- 14 Kirchstetter, T.W. and Thatcher, T.L.: Contribution of organic carbon to wood smoke  
15 particulate matter absorption of solar radiation, *Atmos. Chem. Phys.*, 12, 6067-6072, 2012.
- 16 Koren, I., Martins, J. V., Remer, L. A., and Afargan, H.: Smoke Invigoration Versus Inhibition  
17 of Clouds over the Amazon, *Science*, 321, 946-949, 10.1126/science.1159185, 2008.
- 18 Lack, D.A., Lovejoy, E.R., Baynard, T., Pettersson, A. and Ravishankara, A.R.: Aerosol  
19 Absorption Measurement using Photoacoustic Spectroscopy: Sensitivity, Calibration, and  
20 Uncertainty Developments, *Aerosol Sci. Technol.*, 40, 697-708, 2006.
- 21 Lambe, A.T., Cappa, C.D., Massoli, P., Onasch, T.B., Forestieri, S.D., Martin, A.T., Cummings,  
22 M.J., Croasdale, D.R., Brune, W.H., Worsnop, D.R. and Davidovits, P.: Relationship between  
23 Oxidation Level and Optical Properties of Secondary Organic Aerosol, *Environ. Sci. Technol.*,  
24 47, 6349-6357, 2013.
- 25 Lang-Yona, N., Rudich, Y., Segre, E., Dinar, E. and Abo-Riziq, A.: Complex Refractive Indices  
26 of Aerosols Retrieved by Continuous Wave-Cavity Ring Down Aerosol Spectrometer, *Anal.*  
27 *Chem.*, 81, 1762-1769, 2009.
- 28 Lang-Yona, N., Rudich, Y., Mentel, T.F., Bohne, A., Buchholz, A., Kiendler-Scharr, A., Kleist,  
29 E., Spindler, C., Tillmann, R. and Wildt, J.: The chemical and microphysical properties of  
30 secondary organic aerosols from Holm Oak emissions, *Atmos. Chem. Phys.*, 10, 7253-7265,  
31 2010.
- 32 Liu, P., Zhang, Y. and Martin, S.T.: Complex Refractive Indices of Thin Films of Secondary  
33 Organic Materials by Spectroscopic Ellipsometry from 220 to 1200 nm, *Environ. Sci. Technol.*,  
34 47, 13594-13601, 2013.
- 35 Liu, Y. and Daum, P.H.: Relationship of refractive index to mass density and self-consistency of  
36 mixing rules for multicomponent mixtures like ambient aerosols, *J. Aerosol Sci.*, 39, 974-986,  
37 2008.

- 1 Flores, J.M., Bar-Or, R.Z., Bluvshstein, N., Abo-Riziq, A., Kostinski, A., Borrmann, S., Koren, I.  
2 and Rudich, Y.: Absorbing aerosols at high relative humidity: linking hygroscopic growth to  
3 optical properties, *Atmos. Chem. Phys.*, 12, 5511-5521, 2012.
- 4 Fry, J. L., Kiendler-Scharr, A., Rollins, A. W., Brauers, T., Brown, S. S., Dorn, H. P., Dube, W.  
5 P., Fuchs, H., Mensah, A., Rohrer, F., Tillmann, R., Wahner, A., Wooldridge, P. J., and Cohen,  
6 R. C.: SOA from limonene: role of NO<sub>3</sub> in its generation and degradation, *Atmos. Chem. Phys.*,  
7 11, 3879-3894, 2011.
- 8 Miles, R.E.H., Rudic, S., Orr-Ewing, A.J. and Reid, J.P.: Measurements of the wavelength  
9 dependent extinction of aerosols by cavity ring down spectroscopy, *Phys. Chem. Chem. Phys.*,  
10 12, 3914-3920, 2010.
- 11 Nakayama, T., Matsumi, Y., Sato, K., Imamura, T., Yamazaki, A. and Uchiyama, A.:  
12 Laboratory studies on optical properties of secondary organic aerosols generated during the  
13 photooxidation of toluene and the ozonolysis of  $\alpha$ -pinene, *J. Geophys. Res.-Atmos.*, 115,  
14 D24204, 2010.
- 15 Nakayama, T., Sato, K., Matsumi, Y., Imamura, T., Yamazaki, A. and Uchiyama, A.:  
16 Wavelength Dependence of Refractive Index of Secondary Organic Aerosols Generated during  
17 the Ozonolysis and Photooxidation of alpha-Pinene, *Sola*, 8, 2012.
- 18 Nakayama, T., Sato, K., Matsumi, Y., Imamura, T., Yamazaki, A. and Uchiyama, A.:  
19 Wavelength and NO<sub>x</sub> dependent complex refractive index of SOAs generated from the  
20 photooxidation of toluene, *Atmos. Chem. Phys.*, 13, 531-545, 2013.
- 21 Ng, N.L., Canagaratna, M.R., Zhang, Q., Jimenez, J.L., Tian, J., Ulbrich, I.M., Kroll, J.H.,  
22 Docherty, K.S., Chhabra, P.S., Bahreini, R., Murphy, S.M., Seinfeld, J.H., Hildebrandt, L.,  
23 Donahue, N.M., DeCarlo, P.F., Lanz, V.A., Prévôt, A.S.H., Dinar, E., Rudich, Y. and Worsnop,  
24 D.R.: Organic aerosol components observed in Northern Hemispheric datasets from Aerosol  
25 Mass Spectrometry, *Atmos. Chem. Phys.*, 10, 4625-4641, 2010.
- 26 Ofner, J., Krüger, H. U., Grothe, H., Schmitt-Kopplin, P., Whitmore, K., and Zetzsch, C.:  
27 Physico-chemical characterization of SOA derived from catechol and guaiacol &ndash; a model  
28 substance for the aromatic fraction of atmospheric HULIS, *Atmos. Chem. Phys.*, 11, 1-15,  
29 10.5194/acp-11-1-2011, 2011.
- 30 Park, R.J., Kim, M.J., Jeong, J.I., Youn, D. and Kim, S.: A contribution of brown carbon aerosol  
31 to the aerosol light absorption and its radiative forcing in East Asia, *Atmos. Environ.*, 44, 1414-  
32 1421, 2010.
- 33 Pettersson, A., Lovejoy, E. R., Brock, C. A., Brown, S. S., and Ravishankara, A. R.:  
34 Measurement of aerosol optical extinction at 532nm with pulsed cavity ring down  
35 spectroscopy, *J. Aerosol Sci.*, 35, 995-1011, <http://dx.doi.org/10.1016/j.jaerosci.2004.02.008>,  
36 2004.
- 37 Redmond, H. and Thompson, J.E.: Evaluation of a quantitative structure-property relationship  
38 (QSPR) for predicting mid-visible refractive index of secondary organic aerosol (SOA), *Phys.*  
39 *Chem. Chem. Phys.*, 13, 6872-6882, 2011.

- 1 Rohrer, F., Bohn, B., Brauers, T., Brüning, D., Johnen, F.J., Wahner, A. and Kleffmann, J.:  
2 Characterisation of the photolytic HONO-source in the atmosphere simulation chamber  
3 SAPHIR, *Atmos. Chem. Phys.*, 5, 2189-2201, 2005.
- 4 Rollins, A. W., Kiendler-Scharr, A., Fry, J. L., Brauers, T., Brown, S. S., Dorn, H. P., Dubé, W.  
5 P., Fuchs, H., Mensah, A., Mentel, T. F., Rohrer, F., Tillmann, R., Wegener, R., Wooldridge, P.  
6 J., and Cohen, R. C.: Isoprene oxidation by nitrate radical: alkyl nitrate and secondary organic  
7 aerosol yields, *Atmos. Chem. Phys.*, 9, 6685-6703, 2009.
- 8 Salo, K., Hallquist, M., Jonsson, Å.M., Saathoff, H., Naumann, K.H., Spindler, C., Tillmann, R.,  
9 Fuchs, H., Bohn, B., Rubach, F., Mentel, T.F., Müller, L., Reinnig, M., Hoffmann, T. and  
10 Donahue, N.M.: Volatility of secondary organic aerosol during OH radical induced ageing,  
11 *Atmos. Chem. Phys.*, 11, 11055-11067, 2011.
- 12
- 13 Schnaiter, M., Horvath, H., Möhler, O., Naumann, K.H., Saathoff, H. and Schöck, O.W.: UV-  
14 VIS-NIR spectral optical properties of soot and soot-containing aerosols, *J. Aerosol Sci.*, 34,  
15 1421-1444, 2003.
- 16 Shilling, J.E., Chen, Q., King, S.M., Rosenoern, T., Kroll, J.H., Worsnop, D.R., DeCarlo, P.F.,  
17 Aiken, A.C., Sueper, D., Jimenez, J.L. and Martin, S.T.: Loading-dependent elemental  
18 composition of  $\alpha$ -pinene SOA particles, *Atmos. Chem. Phys.*, 9, 771-782, 2009.
- 19 Spracklen, D.V., Jimenez, J.L., Carslaw, K.S., Worsnop, D.R., Evans, M.J., Mann, G.W., Zhang,  
20 Q., Canagaratna, M.R., Allan, J., Coe, H., McFiggans, G., Rap, A. and Forster, P.: Aerosol mass  
21 spectrometer constraint on the global secondary organic aerosol budget, *Atmos. Chem. Phys.*, 11,  
22 12109-12136, 2011.
- 23 van Krevelen, D.: Graphical-statistical method for the study of structure and reaction processes  
24 of coal, *Fuel*, 24, 269-284, 1950.
- 25 Walser, M.L., Desyaterik, Y., Laskin, J., Laskin, A. and Nizkorodov, S.A.: High-resolution  
26 mass spectrometric analysis of secondary organic aerosol produced by ozonation of limonene,  
27 *Phys. Chem. Chem. Phys.*, 10, 1009-1022, 2008.
- 28 Washenfelder, R.A., Flores, J.M., Brock, C.A., Brown, S.S. and Rudich, Y.: Broadband  
29 measurements of aerosol extinction in the ultraviolet spectral region, *Atmos. Meas. Tech.*, 6,  
30 861-877, 2013.
- 31 Wex, H., Petters, M.D., Carrico, C.M., Hallbauer, E., Massling, A., McMeeking, G.R., Poulain,  
32 L., Wu, Z., Kreidenweis, S.M. and Stratmann, F.: Towards closing the gap between hygroscopic  
33 growth and activation for secondary organic aerosol: Part 1 – Evidence from measurements,  
34 *Atmos. Chem. Phys.*, 9, 3987-3997, 2009.
- 35 Wiedensohler, A.: An approximation of the bipolar charge distribution for particles in the  
36 submicron size range, *J. Aerosol Sci.*, 19, 387-389, 1988.
- 37 Yu, Y., Ezell, M.J., Zelenyuk, A., Imre, D., Alexander, L., Ortega, J., D'Anna, B., Harmon,  
38 C.W., Johnson, S.N. and Finlayson-Pitts, B.J.: Photooxidation of  $\alpha$ -pinene at high relative

1 humidity in the presence of increasing concentrations of NO<sub>x</sub>, *Atmos. Environ.*, 42, 5044-5060,  
2 2008.

3 Zhao, W., Dong, M., Chen, W., Gu, X., Hu, C., Gao, X., Huang, W. and Zhang, W.:  
4 Wavelength-resolved optical extinction measurements of aerosols using broad-band cavity-  
5 enhanced absorption spectroscopy over the spectral range of 445–480 nm, *Anal. Chem.*, 85,  
6 2260-2268, 2013.

7

8

9

10

11



**Table 1.** Description of the experiments performed in this study

<b>Experiment</b>	<b>Description</b>	<b>VOC (ppb)</b>	<b>Initial [OH] (<math>\times 10^6</math> molec. cm<sup>-3</sup>)</b>	<b>[NO<sub>x</sub>] (ppbv)</b>	<b>Local time experiments began</b>	<b>Total duration</b>
BVOCs	BVOCs mix only	$\alpha$ -pinene, limonene (48, 48)	7.4	< 0.25	11:30	~50 h.
Sequential	BVOCs mix & p-xylene-d <sub>10</sub> (p-xylene-d <sub>10</sub> added 5h after BVOCs mix)	$\alpha$ -pinene, limonene (39, 39) p-xylene-d <sub>10</sub> (51)	7.8	< 0.30	11:37	~ 29 h.
Mixture	BVOCs mix & p-xylene-d <sub>10</sub> (added together)	$\alpha$ -pinene, limonene (42, 42) p-xylene-d <sub>10</sub> (90)	8.0	< 0.25	11:33	~ 29.5 h.

**Table 2.** Real parts of the RI for different O / C ratios in this study compared with literature values

Real part (n) of the RI	O/C atomic ratio	VOC (Initial conc. in ppmv)	SOA formation	Ini. [O <sub>3</sub> ] (ppmv)	Ini. [OH] (×10 <sup>10</sup> molec. cm <sup>-3</sup> )	Exposure time	Wavelength (nm)	Reference
1.50(±0.01) – 1.49(±0.01)	0.37 – 0.38	α-pinene + limonene (0.048 + 0.048)	ozonolysis and OH oxidation	0.2	0.00074	up to 50 h	405	This work
1.46(±0.01) – 1.50(±0.02)	0.39 – 0.44	α-pinene + limonene + p-xylene-d <sub>10</sub> <sup>a</sup> (0.039 + 0.039 + 0.051)	ozonolysis and OH oxidation	0.2	0.00078	up to 29 h	405	This work
1.46(±0.01) – 1.51(±0.01)	0.35 – 0.42	α-pinene + limonene + p-xylene-d <sub>10</sub> (0.042 + 0.042 + 0.090)	ozonolysis and OH oxidation	0.2	0.00080	up to 29.5 h	405	This work
1.511 (±0.003)	< 0.3	α-pinene (4.0±1.4) <sup>b</sup>	ozonolysis	52.2±2.2 <sup>b</sup>	Scavenger <sup>c</sup>	~38 sec	405	Liu et al. (2013)
1.514 (±0.003)	< 0.3	limonene (3.0)	ozonolysis	30±0.5			405	Liu et al. (2013)
1.51(±0.02) - 1.45(±0.04)	0.42 – 0.93	α-pinene (NA)	OH oxidation	NA	22(±11) – 150(±20)	~100 sec.	405	Lambe et al. (2013)
1.66(±0.04) – 1.58(±0.06)	0.52 – 1.29	naphthalene (NA)	OH oxidation	NA			405	Lambe et al. (2013)
1.55(±0.01) – 1.53(±0.01)	0.70 – 1.14	guaiacol (NA)	OH oxidation	NA			405	Lambe et al. (2013)
1.54(±0.01) – 1.48(±0.01)	0.37 – 0.89	tricycle[5.2.10 <sup>2,6</sup> ]decane (NA)	OH oxidation	NA			405	Lambe et al. (2013)
1.449(±0.030) – 1.567(±0.043)	0.64 – 0.73	toluene (4.0)	photooxidation	NA	~27	up to 4 h	405	Nakayama et al. (2013)
1.431(±0.026) – 1.498(±0.025)	0.64 – 0.73	toluene (4.0)	photooxidation	NA			532	Nakayama et al. (2013)
1.475(±0.022) – 1.498(±0.030)	0.43 – 0.47	α-pinene (0.1)	ozonolysis and photooxidation	1.1 and 2.6	~27	up to 4 h	405	Nakayama et al. (2012)
1.476(±0.021) – 1.458(±0.02)	0.43 – 0.47	α-pinene (0.1)	ozonolysis and photooxidation				532	Nakayama et al. (2012)
1.47(±0.02) – 1.52(±0.00)	0 – 0.35	squalene (NA)	OH oxidation	NA	0 – ~200	37 sec.	532	Cappa et al. (2011)
1.47(±0.02) – 1.54(±0.00)	0.45 – 0.75	azelaic acid (NA)	OH oxidation				532	Cappa et al. (2011)

<sup>a</sup>p-xylene-d<sub>10</sub> was added 5h after; <sup>b</sup>Average of four experiments; <sup>c</sup>Butanol was used as an OH scavenger; NA: not available



**Instrumentation**

Temperature, Relative humidity	SMPS	BBCES
[O <sub>3</sub> ], NO and NO <sub>2</sub> monitors	CPC	VTDMA
Spectral radiometer	PTR-MS	HR-ToF-AMS

**Figure 1.** Schematic of the experimental procedure and instrumentation used for measuring the evolution of secondary organic aerosol over a diurnal cycle. All experiments began around 11:30 hrs. local time.

Acronyms:

SMPS – Scanning mobility particle sizer

CPC – Condensation particle counter

PTR-MS – Proton transfer reaction - mass spectrometer

BBCES – Broadband cavity enhanced spectrometer

VTDMA – Volatility tandem differential mobility analyser

HR-ToF-AMS – High resolution – time of flight – aerosol mass spectrometer

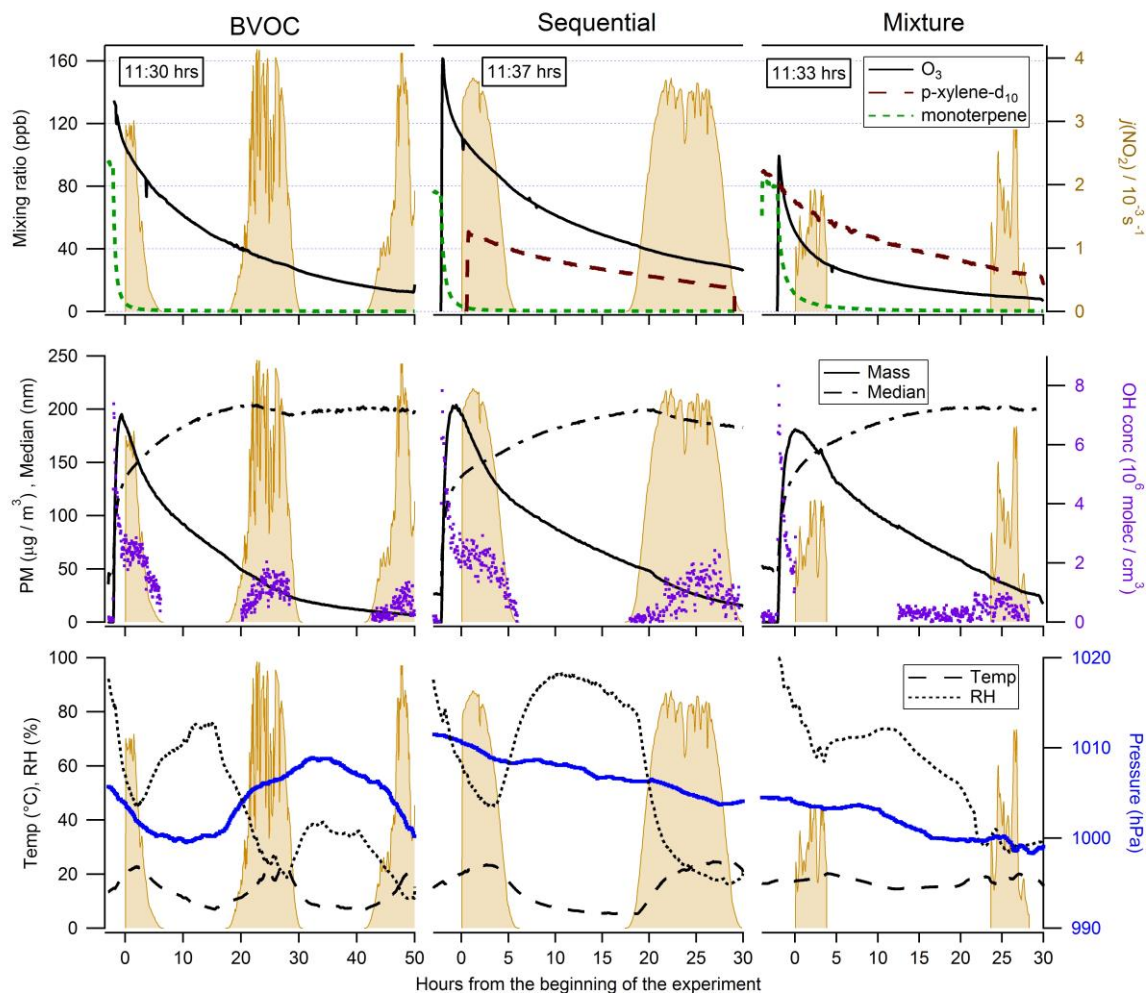


**Figure 2.** Time series of the three experiments performed. The BVOC experiment is shown in the left panel, the sequential experiment in the middle panel, and the mixture experiment is shown in the right panel. The mixing ratio of ozone (black line), the mixture of  $\alpha$ -pinene and limonene (monoterpenes; dotted green line), and p-xylene-d<sub>10</sub> (red dashed line) are shown in the top panels. The total mass (black line), median diameter (black dash-dot line), and OH concentration (purple dots) are shown in the middle panels. The temperature (black dash line), relative humidity (black dotted line), and pressure (blue dots) are shown in the lower panels. The photolysis rates of NO<sub>2</sub> (orange area) are presented in all panels to indicate the diurnal cycles; the rate values are shown in the right top axis. NO<sub>x</sub> levels were below 1ppbv and are not shown here. The local time at which each experiment began is shown in the top panels.

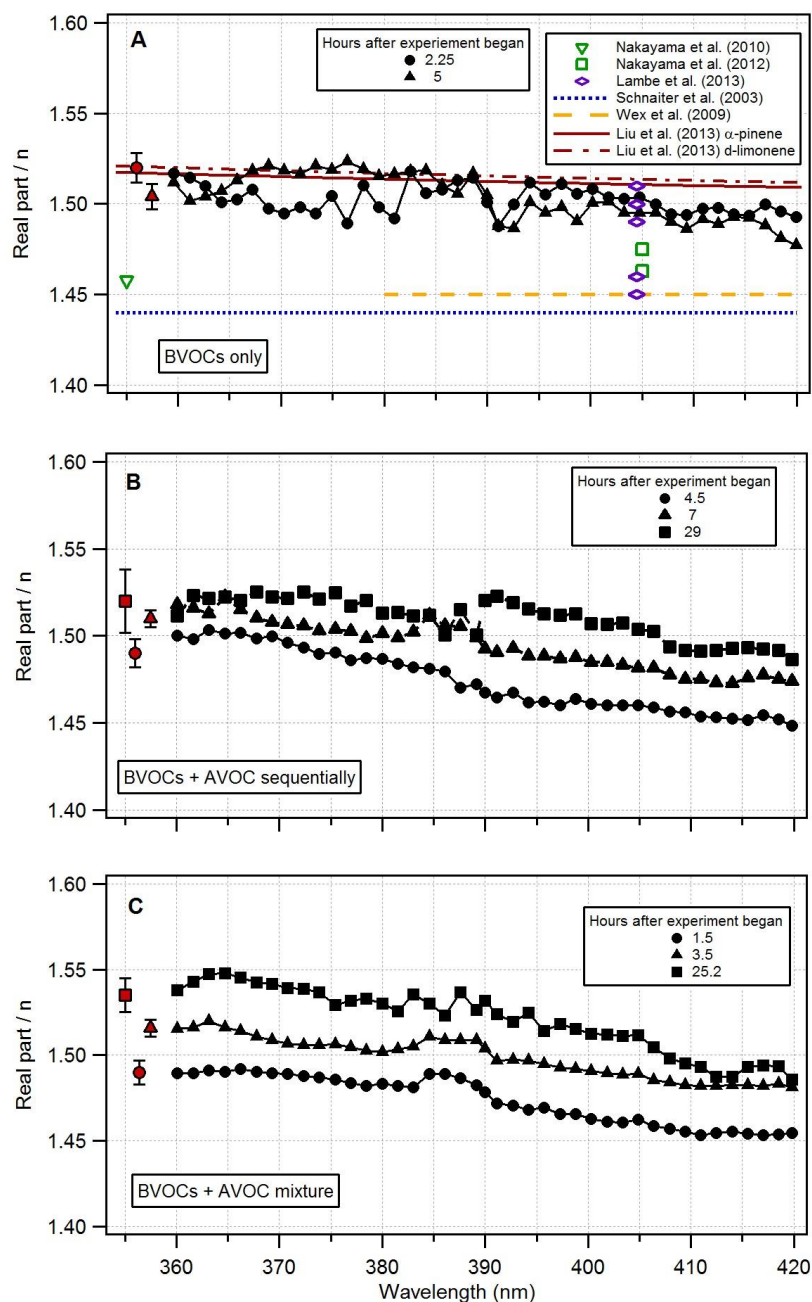


**Figure 3.** Change of the real part of the complex refractive index vs. wavelength as a function of time for SOA produced from (A) only a mixture of  $\alpha$ -pinene and limonene, compared to literature values of the real RI of  $\alpha$ -pinene; (B) a mixture of  $\alpha$ -pinene and limonene followed by the addition of p-xylene-d<sub>10</sub> 5 h after, and (C) a mixture of  $\alpha$ -pinene, limonene and p-xylene-d<sub>10</sub> (only 3 retrievals are shown for clarity). The averaged error bars of the retrieved RI values are shown as the red markers on the left for clarity. The average errors for the retrievals in (A) are:  $0.008(\pm 0.008)$ , and  $0.006(\pm 0.005)$  for 2.25 h and 5 h, respectively. The average errors for the retrievals in (B) are:  $0.005(\pm 0.008)$ ,  $0.004(\pm 0.001)$ , and  $0.018(\pm 0.007)$  for 4.5 h, 7 h, and 29 h, respectively. The average errors for the retrievals in (C) are:  $0.007(\pm 0.006)$ ,  $0.004(\pm 0.003)$ , and  $0.010(\pm 0.004)$  for 1.5 h, 7 h, and 25.2 h, respectively.

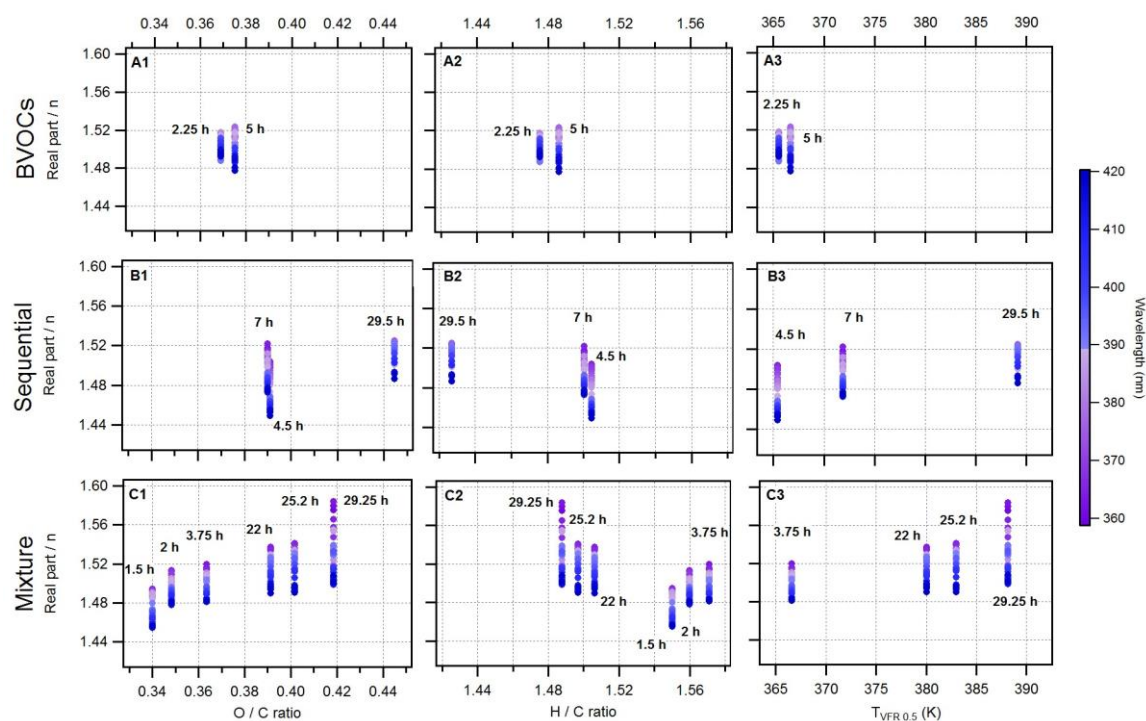


**Figure 4.** The change in time (given in hours, shown next to the retrieved values) for the retrieved real part of the RI as a function of O / C ratio (panels A1, B1 and C1), H / C ratio (panels A2, B2 and C2), and  $T_{VFR\ 0.5}$  (the temperature at which the volume fraction remaining was reduced by half, panels A3, B3 and C3). The top panels – A1, A2 and A3 – show the results for the SOA produced from a 1 to 1 mixture of  $\alpha$ -pinene and limonene. The middle panels – B1, B2, and B3 – show the results for the SOA produced from the mixture of  $\alpha$ -pinene, limonene, and p-xylene-d<sub>10</sub>. The lower panels – C1, C2, and C3 – show the results for the SOA produced from the sequential addition of the mixture of  $\alpha$ -pinene and limonene followed by p-xylene-d<sub>10</sub>. The color scale indicates the measured wavelength. The error bars for the O/C (31%), H/C (10%), and  $T_{VFR\ 0.5}$  are not shown for clarity. The average error for the  $T_{VFR\ 0.5}$  is 2.3 K.

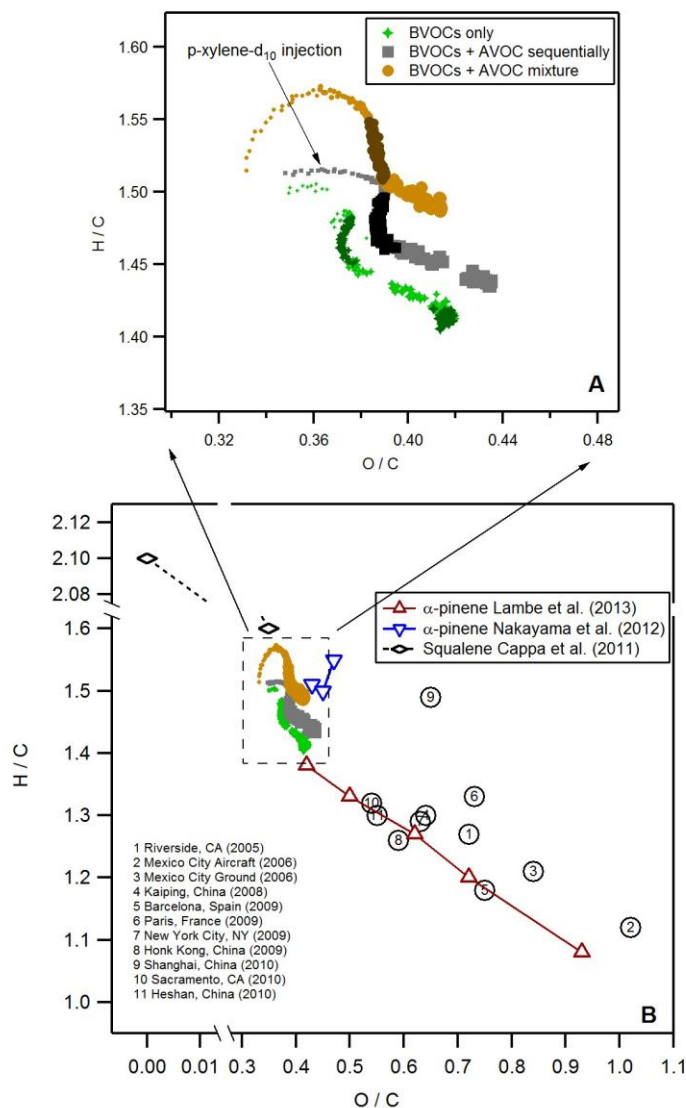


**Figure 5.** Van Krevelen diagram showing the ratio of H/C to O/C measured for the three experiments performed in this study: a mixture of  $\alpha$ -pinene with limonene (green diamonds), a mixture of  $\alpha$ -pinene with limonene with a sequential addition of p-xylene-d<sub>10</sub> (grey squares), and a mixture of  $\alpha$ -pinene, limonene and p-xylene-d<sub>10</sub> (orange circles). The change in marker size depicts time; smaller markers refer to the beginning of the experiment, and larger markers to the end. The top panel (A) shows specifically the three experiments performed in this study. The darker colours depict night time. In the lower panel (B), the results are compared to the low volatility oxygenated organic aerosol factors from HR-AMS field campaigns (numbered circles, adopted from Daumit et al. (2013)), results for  $\alpha$ -pinene SOA from Lambe et al. (2013) (red triangles), and Nakayama et al. (2012) (blue inverted triangles), and squalene SOA from Cappa et al. (2011) (black rhombus).



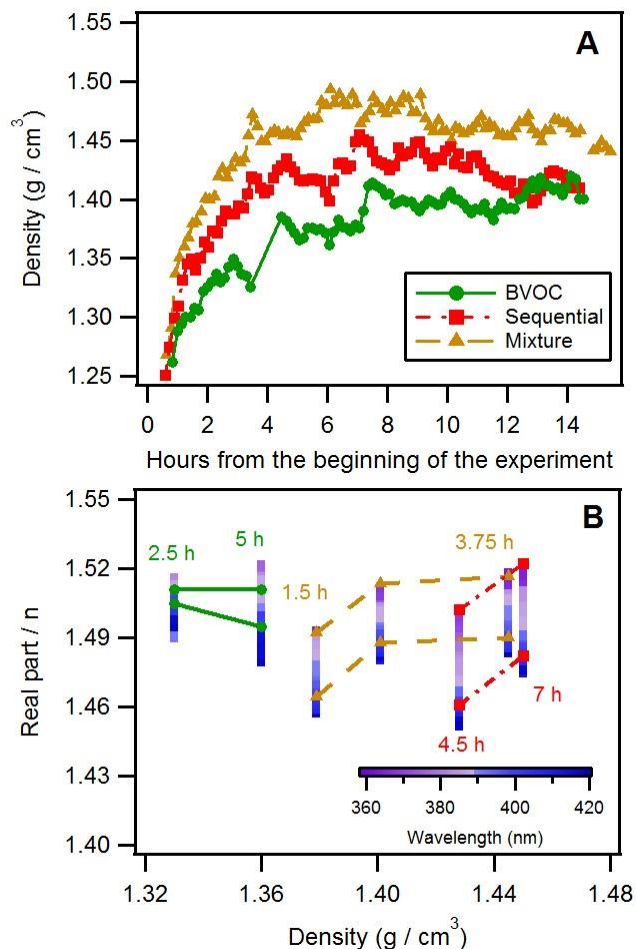


**Figure 6.** A) Time series of the density measured for the BVOC (green circles), the sequential (red squares); and the mixture (orange triangles) experiment. B) The change in time of the real part of the RI vs. density for each experiment performed. The colour bars show the span in the RI for the wavelengths measured, the time span between the measurements is written above (for the BVOC and sequential experiments) and below (the mixture experiment) each set of measurements.



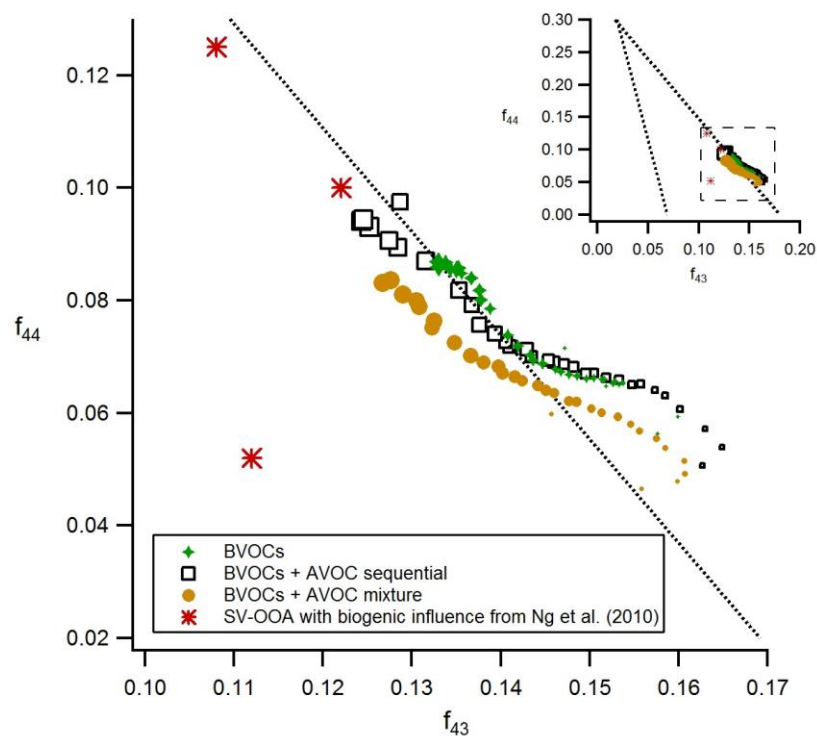


**Figure 7.**  $f_{44}$  vs.  $f_{43}$  for the SOA produced from the mixture of  $\alpha$ -pinene and limonene (green diamonds), from the sequential addition of the mixture of  $\alpha$ -pinene and limonene followed by p-xylene- $d_{10}$  (black squares), and from the mixture of  $\alpha$ -pinene, limonene, and p-xylene- $d_{10}$  (orange circles). The change in size of the markers depicts time; smaller markers refer to the beginning of the experiment, and larger markers to the end. The insert shows the total triangular area (dotted lines) that represents the common values of ambient oxygenated organic aerosol components, adapted from Ng et al. (2010).